# Nanoscale

Accepted Manuscript


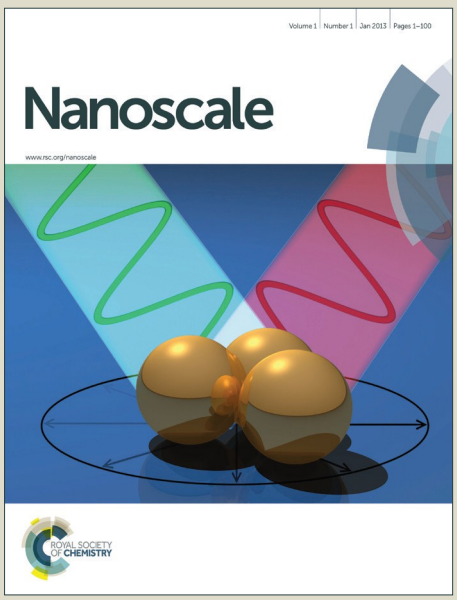





ROYAL SOCIETY OF CHEMISTRY

www.rsc.org/nanoscale

Journal Name

ARTICLE

# Rational design of hierarchically-structured $CuBi_2O_4$ composites by deliberate manipulation of the nucleation and growth kinetics of $CuBi_2O_4$ for environmental applications

Received 00th January 20xx,
Accepted 00th January 20xx

DOI: 10.1039/x0xx00000x

www.rsc.org/

Wen-Da Oh[a, b], Shun-Kuang Lua[a, c], Zhili Dong[a, c], Teik-Thye Lim[a, b*]

A versatile eco-friendly synthesis scheme was developed to fabricate a series of hierarchically-structured $CuBi_2O_4$ composites for environmental applications. By simple tuning of the synthesis protocol (i.e. controlling the ethylene glycol to water ratio in the reaction matrix and employing different auxiliary metal precursors consisting of either $Cu^{2+}$, $Co^{2+}$ or $Fe^{3+}$ species), deposition of various metal oxides on $CuBi_2O_4$ was achieved. The proposed one-pot synthesis protocol utilizes the fast nucleation and controlled growth kinetics of the $CuBi_2O_4$ to deliberately immobilize the desired metal oxides on the surface of the $CuBi_2O_4$. The manipulations of the diffusion rate, mass transfer kinetics and atomic mobility of the metal precursors by controlling the viscosity and dielectric property of the reaction matrix lead to the formation of different $CuBi_2O_4$ composites with desired properties. The synergistic coupling effect between the $CuBi_2O_4$ and deposited metal oxide contributed to the superior performance of the novel $CuBi_2O_4$ composites. The $CuBi_2O_4$ composites demonstrate excellent potential for various environmental applications such as being a catalyst for generating sulfate radicals from peroxymonosulfate for organic pollutant removal in water and being a disinfectant. The proposed green synthesis protocol is simple and offers flexibility for fabricating hierarchically-structured $CuBi_2O_4$ composites with enhanced properties for targeted applications.

## 1. Introduction

Self-assembled nanomaterials have broad prospects in water remediation [1]. Recently, continuous efforts have been made to employ hierarchically-structure nanomaterials for environmental applications [2]. In particular, the Bi-based nanomaterials provide an attractive avenue for water treatment due to its attractive multifunctional capabilities (i.e. as photocatalyst, adsorbent, Fenton catalyst, electrochemical oxidation electrode etc.) [3-5]. The Bi-based nanomaterials have a high density of surface hydroxyl groups which can act as a platform for synergistic coupling with other metal oxides for performance enhancement [6].

To date, there are various reports on the promising use of $CuBi_2O_4$ composites for various applications including photoelectrochemical application [7-9], water splitting [10-13], electrochemical capacitors [14], sulfate radical generation [15] and photocatalysis [16-26]. These studies also demonstrated that $CuBi_2O_4$ exhibited poor performance on its own but could have attractive synergistic effect and heterojunction when coupled with other metal oxides. Most of the fabrication protocols involve a multistep synthesis approach, high-energy and/or environmentally-harmful chemicals. Moreover, the fabrication protocols in the literature are only limited to a single type $CuBi_2O_4$ composite. Without good control and understanding of the synthesis conditions, it is challenging to fabricate a high performance $CuBi_2O_4$ composite using a single-step method due to several drawbacks such as the (i) ease of $CuBi_2O_4$ to grow isotropically which may lead to its decrease in performance, (ii) difficulty of other metal oxides to be deposited on $CuBi_2O_4$ under different conditions, and (iii) formation of undesirable phases.

Therefore, the development of an eco-friendly, low-cost but versatile synthesis strategy that can be used to fabricate different types of hierarchically-structured $CuBi_2O_4$ composites is highly desirable. The synthesis protocol in this study is designed to be eco-friendly by avoiding the use of hazardous chemicals/solvents. The hydrothermal method is widely used for green synthesis by many researchers [27, 28]. To engineer different $CuBi_2O_4$ composites, the ethylene glycol (EG) was selected as a green co-solvent to manipulate the mass transfer rate, diffusion kinetics and atomic mobility of the metal

[a] Nanyang Environment and Water Research Institute (NEWRI), Interdisciplinary Graduate School (IGS), Nanyang Technological University, 1 Cleantech Loop, CleanTech One, Singapore 637141, Singapore.
[b] Division of Environmental and Water Resources Engineering, School of Civil and Environmental Engineering, Nanyang Technological University, 50 Nanyang Avenue, Singapore 639798, Singapore.
[c] School of Materials Science and Engineering, Nanyang Technological University, 50 Nanyang Avenue, Singapore 639798, Singapore.
[d] *Corresponding author. Tel: +65-6790 6933, Fax: +65-6791 0676,
[e] E-mail address: cttlim@ntu.edu.sg (Lim T.T.)Electronic Supplementary Information (ESI) available: (i) The FESEM micrographs of the $CuBi_2O_4$ synthesized at 140°C and at $Cu^{2+}$:$CuBi_2O_4$ of 0.5:1, (ii) EDX elemental mappings of various $CuBi_2O_4$ composites, (iii) FESEM micrographs and XRD patterns of the $CuBi_2O_4$ composites with $Cu_2O$ phase, and (iv) The FESEM micrograph and XRD pattern of $CuBi_2O_4$ composite synthesized with $Fe^{3+}$:$CuBi_2O_4$ of 0.25:1 at EG:water ratio of 1:2.
[f] . See DOI: 10.1039/x0xx00000x

precursors by deliberate tuning of the viscosity and dielectric property of the reaction matrix [29, 30]. This also allows control of the nucleation and growth rates of $CuBi_2O_4$ and metal oxides.

Herein, a one-pot hydrothermal synthesis is proposed as an eco-friendly synthesis method to fabricate various three-dimensional hierarchically-structured $CuBi_2O_4$ composites for environmental applications. The synthesis protocol demonstrated excellent versatility for depositing various $Fe^{3+}$-, $Co^{2+}$- and $Cu^{2+}$-transition metal oxides on the surface of $CuBi_2O_4$ for various targeted applications. The fabricated $CuBi_2O_4$ composites were evaluated for environmental applications such as generating sulfate radicals from peroxymonosulfate (PMS) for ultrafast degradation of organic pollutant and disinfection of *E. coli*.

## 2. Experimental

### 2.1 Materials

The chemicals used in this study are of analytical grade. The chemicals used are $Cu(NO_3)_2{\cdot}3H_2O$ (Qrëc™), $Co(NO_3)_2{\cdot}6H_2O$ (Alfa Aesar), $Fe(NO_3)_3{\cdot}9H_2O$ (Merck), $Bi(NO_3)_3{\cdot}5H_2O$ (Alfa Aesar), NaOH (Alfa Aesar), nitric acid (Merck), acetonitrile (Merck), KI (Fisons), NaCl (Qrëc™), PMS (in the form of commercially-available Oxone®, $2KHSO_5{\cdot}KHSO_4{\cdot}K_2SO_4$, Alfa Aesar), sulfanilamide (Sigma-Aldrich), sulfacetamide (Sigma-Aldrich), sulfathiazole (Sigma-Aldrich), sulfamethoxazole (Sigma-Aldrich), benzotriazole (Alfa Aesar) and bisphenol A (Merck). All the experiments were conducted using the deionized (DI) water (18.2 MΩ cm).

### 2.2 Synthesis of $CuBi_2O_4$ composites

The $CuBi_2O_4$ composites were fabricated using a facile one-step hydrothermal synthesis. In a typical procedure, 2 mmol of $Cu(NO_3)_2{\cdot}3H_2O$, 4 mmol of $Bi(NO_3)_3{\cdot}5H_2O$ and 0.5 mmol of auxiliary metal precursor consisting of either $Cu(NO_3)_2{\cdot}3H_2O$, $Fe(NO_3)_3{\cdot}9H_2O$ or $Co(NO_3)_2{\cdot}6H_2O$ were dissolved in 50 mL of 0.5 M $HNO_3$ (denoted as solution A). After rapid magnetic stirring of solution A for 1 h, 25 mL of 2 M NaOH in (25-x) mL of water and x mL of EG was gradually added. The resultant solution was stirred for another 6 h. Then, the solution was transferred into a 125-mL Teflon-line stainless steel autoclave and heated at 200 °C for 12 h in an oven. The resultant solid product was collected, washed several times with deionized water and freeze-dried. The synthesis condition of the $CuBi_2O_4$ composites, BET specific surface area and material phases are presented in Table 1. The $CuBi_2O_4$ composites prepared with auxiliary $Cu^{2+}$, $Co^{2+}$ and $Fe^{3+}$ at 0.25 metal to 1 $CuBi_2O_4$ ratio without EG are denoted as CuO-CuB, CoO-CuB and FeO-CuB, respectively, while those prepared with EG:water ratio of 1:11.5 are denoted as CuO-CuB-EG, CoO-CuB-EG and FeO- CuB -EG, respectively. The $CuBi_2O_4$ composites prepared with auxiliary $Cu^{2+}$, $Co^{2+}$ and $Fe^{3+}$ at 0.25 metal to 1 $CuBi_2O_4$ and EG:water ratio of 1:2 are denoted as CuO-CuB-EG2, CoO-CuB-EG2 and FeO- CuB –EG2, respectively, while the $CuBi_2O_4$ composites prepared with $Cu^{2+}$:$CuBi_2O_4$ ratio of 0.5:1 and 1:1 (with EG:water ratio of 1:11.5) are denoted as CuO2-CuB-EG and CuO3-CuB-EG, respectively.

### 2.3 Characterization study

The SEM micrographs and EDX mappings of the $CuBi_2O_4$ composites were obtained using a FESEM (JEOL JSM 7600F) equipped with EDX (Oxford Xmax80 LN2 Free). The XRD patterns were obtained using a X-ray diffractometer (Bruker AXS D8 Advance, with 0.02° $s^{-1}$ scan rate) operating under 40 kV and 40 mA with X-ray source of Cu-Kα ($\lambda$ = 1.5418 Å). The specific surface area of the $CuBi_2O_4$ composites were calculated from the $N_2$ adsorption–desorption isotherm at 77 K (Quantachrome Autosorb-1 Analyzer).

### 2.4 Performance evaluation

The performance of the $CuBi_2O_4$ composites as PMS activator was evaluated in a batch experiment with sulfanilamide as the target pollutant [31]. Sulfanilamide, which is a sulfonyl antibiotic, is chosen as a model pollutant due to its widespread use. Water pollution due to the sulfonyl drugs can induce antibiotic resistance bacteria. In a typical experiment, a solution containing PMS and 2.5 mg $L^{-1}$ of sulfanilamide was prepared. Then, 0.2 g $L^{-1}$ of $CuBi_2O_4$ composite was added into the solution and sampling of the aliquots was carried out at selected time intervals. The aliquots were filtered, quenched with methanol, and sulfanilamide concentration was analyzed using high performance liquid chromatography (HPLC). The effects of pH, catalyst loading and PMS dosage were investigated for the best performing $CuBi_2O_4$ composite. Degradation of other priority pollutants (i.e. sulfacetamide, sulfamethoxazole, sulfathiazole, benzotriazole and bisphenol A) was also investigated at the optimum condition with the best performing $CuBi_2O_4$ composite. The concentrations of SA, sulfacetamide, sulfamethoxazole, sulfathiazole and benzotriazole were quantified from a calibration curve with HPLC operated under the following conditions: reverse phase column (Hypersil Gold) with 70:30 water to acetonitrile ratio and a UV detector at $\lambda_{max}$ = 260 nm. The bisphenol A was quantified from a calibration curve with HPLC operated under the following conditions: reverse phase column (Hypersil Gold) with 40:60 water to acetonitrile ratio and a UV detector at $\lambda_{max}$ = 220 nm.

The antibacterial property of the $CuBi_2O_4$ composites (i.e.: CuO-CuB, CuO-CuB-EG, CuO2-CuB-EG and CuO3-CuB-EG) were evaluated using the spread plate technique. The *Escherichia coli* (*E. coli*, K12 ER2925, New England Biolab), a major group of gram-negative bacteria, was selected as the model pathogen. In a typical experiment, *E. coli* was incubated in a Luria-Bertani solution for at least 24 h at 37°C. Then, the *E. coli* was purified by repeated centrifugation and resuspension into 0.85% NaCl solution. The *E. coli* cell density was adjusted to 3 ×$10^7$ cfu $mL^{-1}$. To investigate the antibacterial property of selected $CuBi_2O_4$ composites, selected concentration of *E. coli* was spread on the Luria-Bertani agar plate and the number of colonies formed before and after 2 h contact with selected $CuBi_2O_4$ composites was compared.

Journal Name

ARTICLE

**Table 1**: Synthesis conditions, crystal phase, BET surface area and potential environmental applications of the $CuBi_2O_4$ composites prepared using the versatile hydrothermal method.

| $CuBi_2O_4$ composites | Ratio of auxiliary metal precursor to $CuBi_2O_4$ | EG:water ratio | Mineral phases | BET surface area ($m^2/g$) | Potential environmental application(s) |
|---|---|---|---|---|---|
| CuO-CuB | 0.25 $Cu^{2+}$ to 1 $CuBi_2O_4$ | No EG | $CuBi_2O_4$, CuO | 10.5 | Peroxymonosulfate and persulfate activation. |
| CuO-CuB-EG | 0.25$Cu^{2+}$ to 1 $CuBi_2O_4$ | 1:11.5 | $CuBi_2O_4$, $Cu_2O$ | 6.1 | Disinfection, self-cleaning. |
| CuO2-CuB-EG | 0.5$Cu^{2+}$ to 1 $CuBi_2O_4$ | 1:11.5 | $CuBi_2O_4$, $Cu_2O$ | 6.2 | Disinfection, self-cleaning. |
| CuO3-CuB-EG | 1$Cu^{2+}$ to 1 $CuBi_2O_4$ | 1:11.5 | $CuBi_2O_4$, $Cu_2O$ | 5.2 | Disinfection, self-cleaning. |
| FeO-CuB | 0.25$Fe^{3+}$ to 1 $CuBi_2O_4$ | 1:11.5 | $CuBi_2O_4$, $Fe_2O_3$ | 4.2 | Catalysis. |
| FeO-CuB-EG | 0.25$Fe^{3+}$ to 1 $CuBi_2O_4$ | 1:11.5 | $CuBi_2O_4$, $FeBi_{25}O_{40}$, $Cu_2O$ | 9.3 | Photocatalysis, disinfection, self-cleaning. |
| CoO-CuB | 0.25$Co^{2+}$ to 1 $CuBi_2O_4$ | No EG | $CuBi_2O_4$, CoO | 9.6 | Peroxymonosulfate activation |
| CoO-CuB-EG | 0.25$Co^{2+}$ to 1 $CuBi_2O_4$ | 1:11.5 | $CuBi_2O_4$, CoO | 5.4 | Peroxymonosulfate activation |
| CoO-CuB-EG2 | 0.25$Co^{2+}$ to 1 $CuBi_2O_4$ | 1:2 | $CuBi_2O_4$, Cu, $Bi_2O_3$, $CoBi_{12}O_{20}$ | 8.8 | Peroxymonosulfate activation, disinfection, self-cleaning. |

## 3. Results and discussions

### 3.1 Synthesis and characterization studies

The preliminary study on the time-dependent formation of $CuBi_2O_4$ in **Fig. 1** indicated that the self-assembly of $CuBi_2O_4$ during the hydrothermal process began with the nucleation and crystal growth to form nanorods ($t$<10 min) which might have occurred rapidly. The nanorods then self-assembled under high autogeneous pressure to form a hierarchical microstructure with the lowest Gibbs free energy. The self-assembly process was completed in less than 1 h of the hydrothermal treatment. Subsequently, the hierarchical microstructure further grew and matured via isotropic Ostwald ripening ($t$ = 12 h). Although it was previously reported that the formation of $CuBi_2O_4$ occur through the combination of CuO and $Bi_2O_3$ [32], the rapid formation of $CuBi_2O_4$ suggests that the mechanism of $CuBi_2O_4$ formation could also have proceeded directly from the combination of $Cu(OH)_2$ and $Bi(OH)_3$. The fast $CuBi_2O_4$ formation rate allows the design of various different $CuBi_2O_4$ composites. To prepare various $CuBi_2O_4$ composites using the proposed eco-friendly hydrothermal synthesis scheme, simple manipulation of the reaction condition was conducted by using (i) different auxiliary metal precursors during synthesis (i.e., $Cu^{2+}$, $Fe^{3+}$ and $Co^{2+}$), and (ii) different EG:water ratio (no EG, 1:11.5 and 1:2 v/v).

In the first phase of study, metal oxides with selected transition metal species consisting of either $Cu^{2+}$, $Co^{2+}$ or $Fe^{3+}$ were deliberately anchored onto the $CuBi_2O_4$ surface via the proposed hydrothermal method with water as the solvent to form functional materials with enhanced properties. The schematic illustration of the fabrication of $CuBi_2O_4$ composites via the eco-friendly hydrothermal synthesis scheme is presented in **Fig. 2**. It is postulated that the kinetic factors play a critical role in mediating the formation of the various $CuBi_2O_4$ composites. As the formation of $CuBi_2O_4$ is rapid, the nucleation and crystal growth rates of $CuBi_2O_4$, which could precedes other metal oxides due to its relatively lower free energy barrier, provide an instant platform for other metal oxides to bind onto its surface. The metal oxides could easily anchor and nucleate on the high density surface hydroxyl group found on the fast-forming $CuBi_2O_4$ surface which is facilitated by the formation of $Me_1$-O-$Me_2$ bonds forming $CuBi_2O_4$ composite. Most likely, the process of metal oxide attachment occurs immediately before the self-assembly process but after the formation of $CuBi_2O_4$ nanorods.

**Fig. 3** shows the FESEM micrographs of the as-prepared $CuBi_2O_4$ composites. Various unique $CuBi_2O_4$ composites with sphere-like hierarchical microarchitecture built from sub-units of self-assembled nanorod arrays were obtained with auxiliary $Cu^{2+}$ and $Co^{2+}$ without EG addition (CuO-CuB and CoO-CuB,

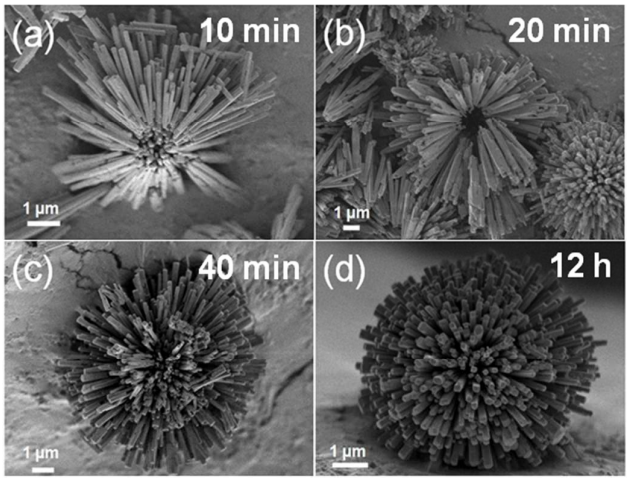


**Fig. 2**: Time-dependent formation of anisotropic $CuBi_2O_4$ at (a) t = 10 min, (b) t = 20 min (c) t = 40 min and (d) t = 12 h. The nucleation and formation of $CuBi_2O_4$ nanorods occurs almost instantly. The ultrafast nucleation and growth kinetics of $CuBi_2O_4$ provides a platform for other metal oxides to attach on its surface.

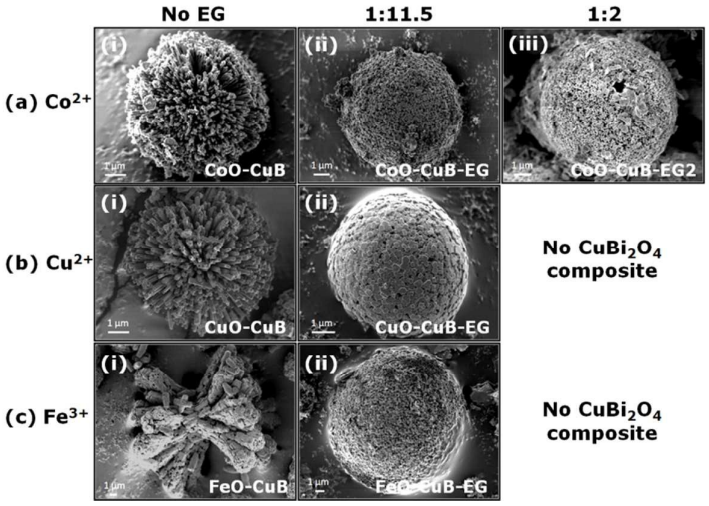


**Fig. 3**: FESEM micrographs of the $CuBi_2O_4$ composites synthesized with various ratios of EG:water. (a) $Co^{2+}$, (b) $Cu^{2+}$, and (c) $Fe^{3+}$.

respectively). The composite fabricated with auxiliary $Fe^{3+}$ (FeO-CuB) has a bow tie-like morphology but with similar sub-units of nanorods. The nanorods have visible nano-particles attached on their surfaces (**Fig. S1**). The reaction temperature, which is an influential kinetic parameter, was kept constant at 200°C throughout this study since synthesis at lower temperature tends to favour anisotropic growth of the $CuBi_2O_4$ (**Fig. S2a**). The optimum ratio of auxiliary metal precursor to $CuBi_2O_4$ is 0.25 to 1 and above this ratio, a mixture of nanorods and nano-particles was obtained (**Fig. S2b**). As the self-assembly process is influenced by many factors (i.e. van der waals forces, hydrophobic interactions, electrostatic and dipolar fields and hydrogen bonds), the difference in the oxidation state of $Fe^{3+}$ (vs. $Co^{2+}$ and $Cu^{2+}$) could have resulted

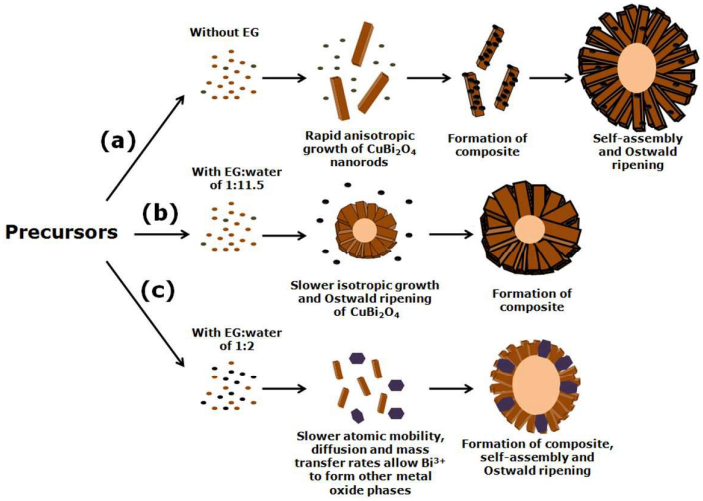


**Fig. 2**: Schematic illustration of the mechanism of formation of $CuBi_2O_4$ composites. (a) Relatively fast nucleation and anisotropic growth of $CuBi_2O_4$ nanorods provide a platform for other metal oxides to anchor and nucleate on its surface. (b) Slower nucleation and isotropic growth of $CuBi_2O_4$ in the EG:water matrix at the ratio of 1:11.5. (c) Further increase in the EG:water ratio to 1:2 allows the formation of other $Bi^{3+}$ oxides which simultaneously grow and self-assembly with $CuBi_2O_4$ resulting in a unique microarchitecture.

in the morphological difference between the composites [33-35].

**Fig. 4** shows the XRD patterns of the as-prepared $CuBi_2O_4$ composites. Except for the distinctive diffraction peaks of $CuBi_2O_4$ (JCPDS file no. 84-1969) in CuO-CuB, CoO-CuB and FeO-CuB, the diffraction peaks of the anchored metal oxides could not be observed because their amounts are rather low compared with that of $CuBi_2O_4$. However, clear difference in diffraction intensity of CuO-CuB, CoO-CuB and FeO-CuB indirectly indicates the compositional difference in the composites. Further analysis with rietveld refinement suggests that some of the transition metals could have also been doped into the Cu sites in $CuBi_2O_4$. The EDX elemental mapping indicates relatively homogeneous distribution of the elements in the $CuBi_2O_4$ composites (**Fig. S3**) further supports the contention above.

In the next phase of study, EG was selected as a green co-solvent to decrease the nucleation and growth kinetics of $CuBi_2O_4$ by varying the viscosity and dielectric property of the reaction matrix during synthesis. The EG has unique intrinsic properties such as it has higher density, more viscous than water and can function as a reducing agent [36]. The EG has also been regarded as a capping agent and has a relatively lower dielectric constant (ε = 37.0, at 20°C) than water (ε = 80.4, at 20°C). It has been reported that by manipulating the viscosity and dielectric constant of the reaction matrix, control of the materials formation kinetics (atomic mobility, diffusion and mass transfer kinetics) can be achieved to obtain the material with desired morphology and crystal phase [37-39]. The calculated viscosities (η) of the EG:water mixtures at 25°C at ratios of 0:1, 1:11.5 and 1:2 are 0.89, 1.40 and 2.45 mPa·s, respectively [40]. The calculated viscosity does not reflect the true viscosity value since it does not include the viscosity change due to the presence of ions (e.g.: metal precursors etc.) in the reaction matrix and it merely provides a semi-

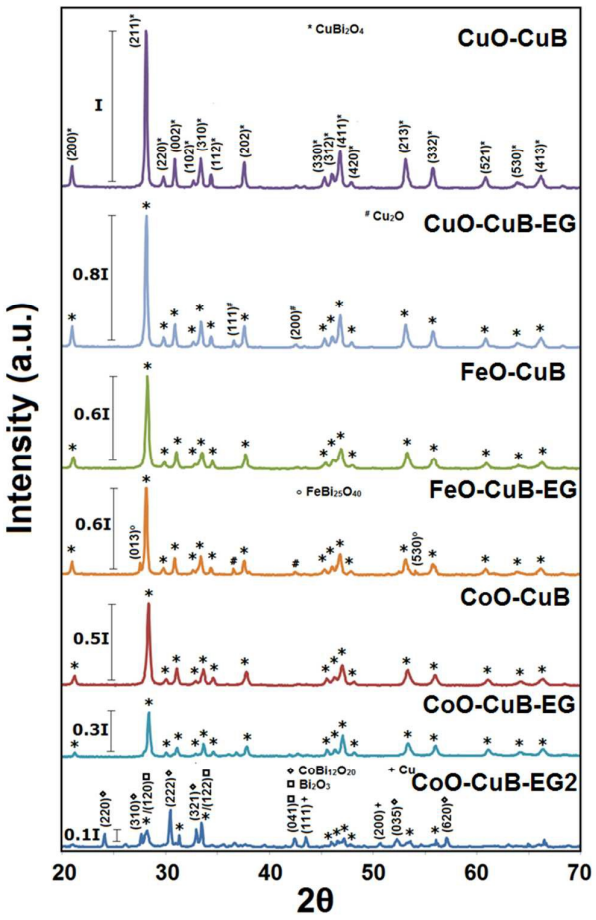


**Fig. 4**: XRD patterns of the $CuBi_2O_4$ composites prepared under various conditions. Although the XRD patterns of CuO-CuB, FeO-CuB and CoO-CuB are similar, the intensities of the diffraction peaks are different indicating the presence of other elements. The presence of EG during synthesis changed the crystal phase of the $CuBi_2O_4$ composite.

quantitative comparison between the systems with and without EG. Two main effects are immediately observed at the EG:water ratio of 1:11.5, namely (i) the change in the morphology, and (ii) the appearance of new crystal phases. The FESEM micrographs (**Fig. 3aii, bii and cii**) and XRD patterns (**Fig. 4**) indicate that new composites were obtained with auxiliary $Cu^{2+}$, $Co^{2+}$ and $Fe^{3+}$ and EG:water ratio of 1:11.5 (denoted as CuO-CuB-EG1, CoO-CuB-EG1 and FeO-CuB-EG1, respectively). These composites have similar pollen-grain-like morphology with characteristic porous surface evidencing the slower $CuBi_2O_4$ growth and isotropic Ostwald ripening processes compared to those prepared without EG addition. The pollen-grain-like morphology is expected at slower $CuBi_2O_4$ growth similar to that when the synthesis was carried out at lower temperature (140°C, **Fig. S2a**). Slower nucleation and growth kinetics tend to favour isotropic growth while faster nucleation and growth kinetics favours anisotropic growth.

The FeO-CuB-EG1 composes of $FeBi_{25}O_{40}$ (JCPDS 46-0416) and $Cu_2O$ (JCPDS 31-1238) phases anchored on the $CuBi_2O_4$ support while CoO-CuB-EG1 has similar XRD pattern as CoO-CuB albeit with lower peak intensity (**Fig. 4**). On the other hand, CuO-CuB-EG1 composes of $Cu_2O$ phase which is the desirable phase with antimicrobial application [41]. The $Cu_2O$ phase is expected based on the reducing property of the EG. The close examination of the FESEM micrographs of CuO-CuB-EG1 indicates that it consists of $Cu_2O$ encapsulating the $CuBi_2O_4$ hollow shell microsphere (**Fig. 5**). Clearly, this imply that the nucleation and growth of $CuBi_2O_4$ takes place before the formation of $Cu_2O$ indicating that the differences between the nucleation and growth rates of $CuBi_2O_4$ and $Cu_2O$ (with EG) is much greater than that of $CuBi_2O_4$ and CuO (without EG). This is because to form $Cu_2O$, $Cu^{2+}$ has to undergo an additional reduction step by EG. Based on the understanding of the mechanism of formation of CuO-CuB-EG1 (and the relatively large differences in formation rate between $Cu_2O$ and $CuBi_2O_4$), further increase of auxiliary $Cu^{2+}$ from $Cu^{2+}$ to $CuBi_2O_4$ ratio of 0.25:1 to 0.5:1 and 1:1 (denoted as CuO2-CuB-EG and CuO3-CuB-EG, respectively) is possible without affecting its morphology. The rietveld refinement of the XRD patterns of CuO-CuB-EG, CuO2-CuB-EG and CuO3-CuB-EG indicates the presence of increasing $Cu_2O$ phase concomitant with the increase of auxiliary $Cu^{2+}$ during synthesis (**Fig. S4**). The disinfection property of $CuBi_2O_4$ composites with $Cu_2O$ was compared in the subsequent section.

It is hypothesize that further reduction in the nucleation and growth kinetics of $CuBi_2O_4$ due to the reduction in atomic mobility of the metal precursors in the reaction matrix will allow the metal precursors (particularly $Bi^{3+}$) to be more readily available to react and form different Bi-based oxides and hence, different $CuBi_2O_4$ composites. To investigate this hypothesis, EG:water ratio of 1:2 was used. No distinctive morphology was observed when EG:water ratio of 1:2 was used for auxiliary $Cu^{2+}$ (0.25 $Cu^{2+}$ to 1 $CuBi_2O_4$) probably due to the intrinsic reduction property of EG which resulted in the two-step further reduction of $Cu^{2+}$ to $Cu^{+}$ and then to Cu. For composites with auxiliary $Co^{2+}$ and $Fe^{3+}$, unique microarchitectures were obtained (denoted as CoO-CuB-EG2 and FeO-CuB-EG2). As predicted, depending on the type of metal precursors present, slower nucleation and growth kinetics of $CuBi_2O_4$ due to the excessive retardation of the atomic mobility of $Bi^{3+}$ allows $Bi^{3+}$ to react with other metal ions to form different material phases (**Fig. 2c**). However, this is also dependent on various factors such as the type of metal present and thermodynamic-feasibility versus the formation of $CuBi_2O_4$. Different material phases have different crystal growth kinetics which could result in different morphologies [42]. The FeO-CuB-EG2 has a unique pollen-grain-like

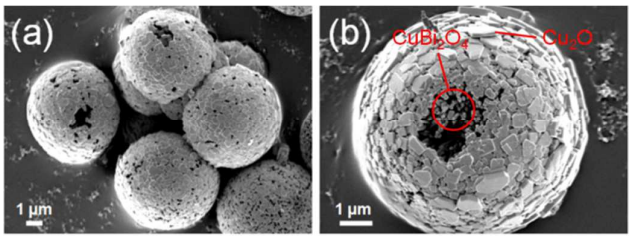


**Fig. 5**: FESEM micrographs of (a) CuO-CuB-EG and (b) incompletely-formed CuO-CuB-EG revealing that the composite consisted of $Cu_2O$ encapsulating the $CuBi_2O_4$.

morphology but however, XRD analysis indicates that it is not a $CuBi_2O_4$ composite (**Fig. S5**) indicating that the $Bi^{3+}$ prefers to form metal oxide phase with $Fe^{3+}$ under this condition. On the other hand, the XRD pattern of CoO-CuB-EG2 in **Fig. 4** can be indexed to $CuBi_2O_4$, Cu, $Bi_2O_3$, $CoBi_{12}O_{20}$ phases. Again, the greater availability of $Bi^{3+}$ at EG:water ratio of 1:2 leads to its reaction with $Co^{2+}$ to form Bi-based metal oxide. The close examination of CoO-CuB-EG2 using SEM reveals that the CoO-CuB-EG2 is composed of a hollow core mesoporous structure with building block consisting of vertically-oriented short $CuBi_2O_4$ nanorods (100-300 nm in length) and hexagonal structure at two different positions, i.e. (i) intercalated between the $CuBi_2O_4$ nanorods and (ii) anchored on the surface of the hollow microsphere (**Fig. 6a and b**). The average wall thickness of CoO-CuB-EG2 is 0.5-1 µm while the hexagonal structure has an average length of ~300 nm and thickness of ~10-20 nm. The nanorods self-assembled to form a hollow microsphere while trapping the other crystal phases into its "shell". Such arrangement of the hollow microsphere gives evidence of the suppression of the nucleation and growth kinetics of $CuBi_2O_4$ resulting in the simultaneous formation of shorter $CuBi_2O_4$ nanorods and other crystal phases. The elemental mapping of the hexagonal structure indicates that it has relatively homogeneous distribution of Cu, Co and Bi elements (**Fig. 6c**).

Based on the results obtained, it can be construed that the following occurs in sequence with decreasing diffusion rate, mass transfer kinetics and atomic mobility of the metal precursors in the reaction matrix during synthesis: anisotropic growth of $CuBi_2O_4$ (fast $CuBi_2O_4$ growth)→ isotropic growth of $CuBi_2O_4$ (slower $CuBi_2O_4$ growth)→ appearance of a new crystal phase due to increase in viscosity and dielectric property of the reaction matrix. The proposed versatile synthesis scheme could be used to fabricate different $CuBi_2O_4$ composites for targeted environmental application with simple manipulation of the reaction condition. It should be emphasized that the one-step synthesis protocol is generally not limited to anchoring a single metal oxide on the $CuBi_2O_4$ surface but could also be used to fabricate $CuBi_2O_4$ composites

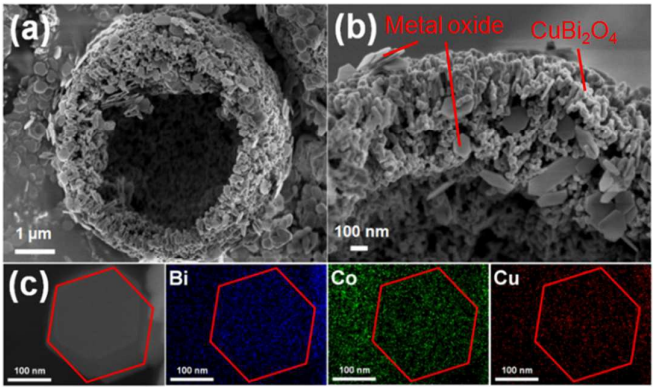


**Fig. 6**: The FESEM micrographs of CoO-CuB-EG2. (a) The deliberately-crushed CoO-CuB-EG2 reveals a hollow inner core. (b) The hexagonal-structured material was found on the surface of $CuBi_2O_4$ and being trapped in the walls of $CuBi_2O_4$ during the self-assembly process. (c) The EDX elemental mappings of the hexagonally-structured material.

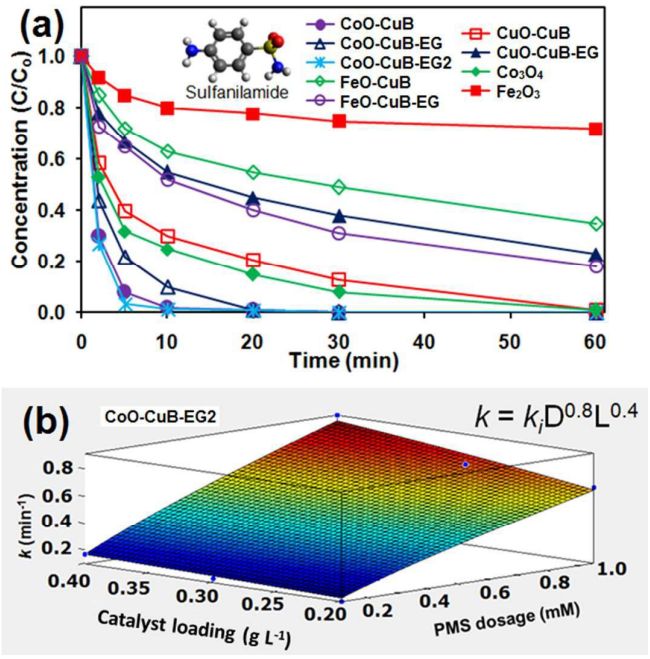


**Fig. 7**: (a) Performance of various $CuBi_2O_4$ composites as PMS activator treating sulfanilamide. Conditions: (a) pH = 7.0, activator loading = 0.2 g $L^{-1}$, PMS dosage = 0.15 g $L^{-1}$, sulfanilamide concentration = 2.5 mg $L^{-1}$, and (b) Relationship between CoO-CuB-EG2 loading (L), PMS dosage (D) and first-order rate constant ($k$).

impregnated with more than one metal oxides (e.g.: CoO-CuB-EG2) or with mixed-metal oxides.

### 3.2 Environmental applications

From the environmental perspectives, the as-prepared $CuBi_2O_4$ composites may have many possible advantages with attractive applications. In this study, the $CuBi_2O_4$ composites were evaluated as PMS activator to generate sulfate radical ($SO_4^{\bullet-}$) for ultrafast sulfanilamide oxidation in water (**Fig. 7a**). The PMS can be activated mainly by the metal oxide anchored on the $CuBi_2O_4$ to produce $SO_4^{\bullet-}$ by the following redox reaction [43]:

$$Me^{n+} + HSO_5^- \rightarrow Me^{(n+1)+} + SO_4^{\bullet-} + H^+ \quad (1)$$

$$Me^{(n+1)+} + HSO_5^- \rightarrow Me^{n+} + SO_5^{\bullet-} + OH^- \quad (2)$$

where Me = transition metal. The generated $SO_4^{\bullet-}$ ($E_o$ = 2.6 V) has a stronger oxidizing power than PMS ($E_o$ = 2.01 V) for sulfanilamide oxidation [31]. Interestingly, most of the as-prepared composites performed significantly better than the commercial activator ($Co_3O_4$) used for this application. The superior performance of the composites is largely attributed to the synergism between the $CuBi_2O_4$ and anchored-metal oxides. To further prove that the synergistic effect exists, the catalytic activities of pure $CuBi_2O_4$, CuO and $CuBi_2O_4$ + CuO mixture were compared with that of the CuO-CuB for the treatment of sulfanilamide via PMS activation (**Fig. S6**). The results indicated that the catalytic activities of $CuBi_2O_4$, CuO and $CuBi_2O_4$-CuO mixture were lower than that of the CuO-CuB further evidencing the synergistic coupling effect. The high surface-hydroxyl groups found on the Bi-based materials could draw the PMS molecule to close proximity with the metal oxide. This important role of surface hydroxyl groups in PMS

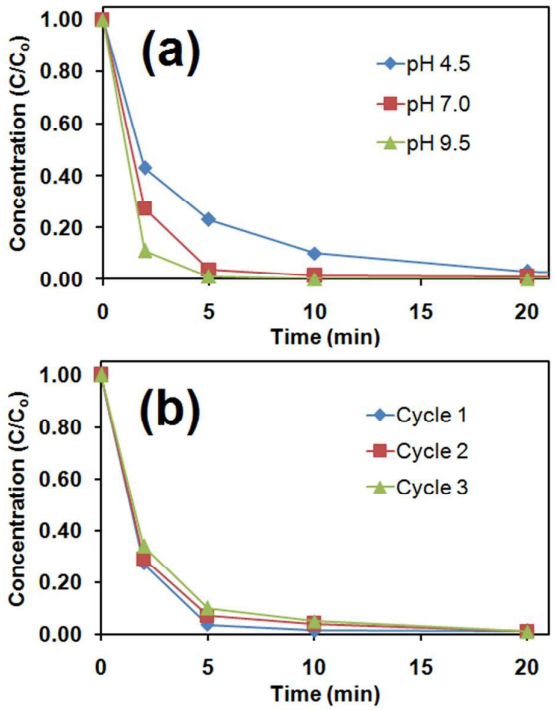


**Fig. 8**: (a) The effect of pH on sulfanilamide degradation and (b) the reusability of CoO-CuB-EG2 over 3 cycles. Conditions: (a) CoO-CuB-EG2 loading = 0.2 g $L^{-1}$, PMS dosage = 0.15 g $L^{-1}$, sulfanilamide concentration = 2.5 mg $L^{-1}$; (b) pH= 7.0, activator loading = 0.2 g $L^{-1}$, PMS dosage = 0.15 g $L^{-1}$, sulfanilamide concentration = 2.5 mg $L^{-1}$.

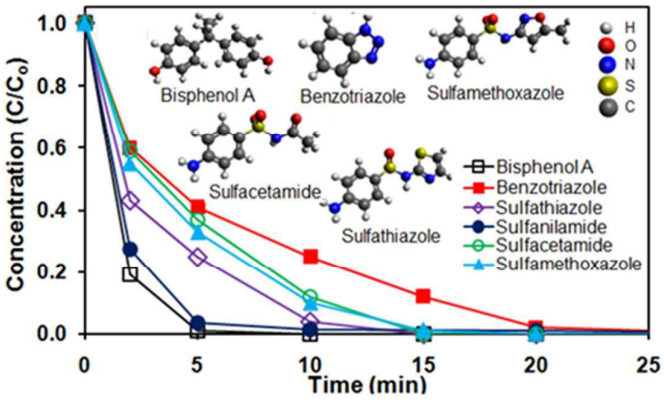


**Fig. 9**: Performance of CoO-CuB-EG2 as PMS activator treating various emerging pollutants. Initial conditions: pH = 7.0, CoO-CuB-EG2 loading = 0.2 g $L^{-1}$, PMS dosage = 0.15 g $L^{-1}$, pollutant concentration = 2.5 mg $L^{-1}$.

activation is also highlighted by several researchers [44, 45]. The metal oxide can then effectively activate the PMS by redox reaction leading to the cleavage of the PMS's peroxide bond to generate $SO_4^{\bullet-}$ for pollutant degradation. The best performing PMS activator is CoO-CuB-EG2 and it was used for further study. The performance of CoO-CuB-EG2 was optimized against pH (**Fig. 8a**), CoO-CuB-EG2 loading and PMS dosage. The relationship of the first-order initial rate constant *k*, CoO-CuB-EG2 loading (L) and PMS dosage (D) at pH 7.0 is as follows: $k = k_i D^{0.8} L^{0.4}$ ($k_i$ = 1.34, $R^2$ = 0.984), where $k_i$ is the intrinsic rate constant (**Fig. 7b**). The CoO-CuB-EG2 could be used for at least

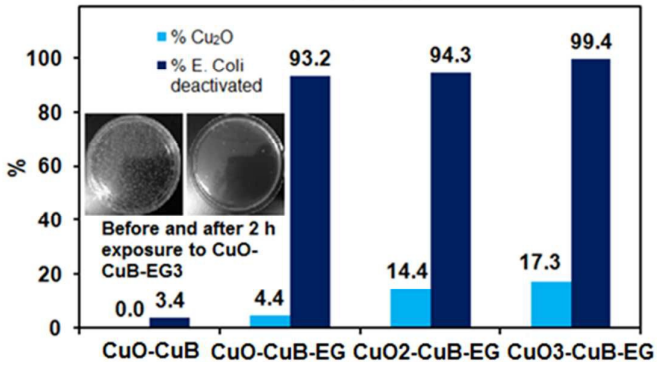


**Fig. 10**: Performance of CuO-CuB, CuO-CuB-EG, CuO2-CuB-EG and CuO3-CuB-EG for the disinfection of *E. coli* with composite loading = 0.25 g $L^{-1}$.

three cycles without deterioration in performance (**Fig. 8b**). The removal of various types of emerging pollutants (sulfacetamide, sulfamethoxazole, sulfathiazole, benzotriazole and bisphenol A) which are considered "high-risk" to human health and the environment via PMS activation by CoO-CuB-EG2 were also evaluated. The CoO-CuB-EG2 is capable of removing these pollutants within 20 min indicating excellent performance of the material (**Fig. 9**).

To further demonstrate the versatility of the synthesis method for preparing functional materials for application in the water treatment, antibacterial composites, namely CuO-CuB-EG, CuO2-CuB-EG and CuO3-CuB-EG were prepared and evaluated for their disinfection property (i.e. disinfection of *E. coli* in water) and the results are presented in **Fig. 10**. The antibacterial activity increased in the following order: CuO-CuB-EG<CuO2-CuB-EG<CuO3-CuB-EG. Typically, the antibacterial activity of $Cu_2O$ is morphology-dependent. The $Cu_2O$ with exposed polar (100) facet has been reported to have an excellent antibacterial property [46, 47]. The CuO-CuB-EG, CuO2-CuB-EG and CuO3-CuB-EG fabricated in this study consists of $CuBi_2O_4$ surrounded by an outer layer of exposed $Cu_2O$ cubic surface (**Fig. 5**). The $CuBi_2O_4$ support provides additional stability and self-cleaning property (i.e. activation of PMS for surface cleaning) to the composites. No significant antibacterial property was observed for CuO-CuB. The main reason for the better disinfection property of CuO-CuB-EG, CuO2-CuB-EG and CuO3-CuB-EG (with $Cu_2O$ phase) compared with CuO-CuB (with CuO phase) is because the $Cu_2O$ has a higher affinity for adsorption and binding with a specific protein in the bacteria which can lead to rapid denaturation of the protein molecule in *E. Coli* [48, 49].

The versatility of the synthesis protocol provides flexibility to design hierarchically-structured $CuBi_2O_4$ composites with high stability and strong performance for water treatment. An additional advantage of the $CuBi_2O_4$ composites is that it has high settling velocity due to the high density of $CuBi_2O_4$ and this allow rapid gravitational settling (within 5 min) for ease of recovery and reuse of the materials.

## Conclusions

In summary, a versatile, one-step hydrothermal synthesis protocol was developed to fabricate $CuBi_2O_4$ composites for various targeted environmental applications. Various $CuBi_2O_4$ composites was fabricated by facile tuning of the (i) auxiliary metal precursors ($Cu^{2+}$, $Co^{2+}$ and $Fe^{3+}$), and (ii) EG:water ratio to control the viscosity and dielectric property of the reaction matrix. The synthesis protocol was developed based on the deliberate kinetic control of the nucleation and growth kinetics of $CuBi_2O_4$ and metal oxide. The $CuBi_2O_4$ can synergistically enhance the performance of other metal oxide when coupled together making it attractive for various environmental applications (e.g. as PMS activator and disinfection).

## Acknowledgements

The financial support from the Academic Research Fund RG76/12 is gratefully acknowledged. The authors would also like to the interdisciplinary graduate school (IGS) and Nanyang Environment and Water Research Institute (NEWRI) for the award of PhD research Scholarship. The kind assistances from all the technical staffs in the Environmental Labs and Facility for analysis characterization testing simulation (FACTS) are deeply appreciated.

## References

[1] S.J. Tesh, T.B. Scott, Advanced Materials 26 (2014) 6056-6068.
[2] Z. Ren, Y. Guo, C.-H. Liu, P.-X. Gao, Frontiers in Chemistry 1 (2013).
[3] Z.-T. Hu, J. Liu, X. Yan, W.-D. Oh, T.-T. Lim, Chemical Engineering Journal 262 (2015) 1022-1032.
[4] S. Wang, Y. Guan, L. Wang, W. Zhao, H. He, J. Xiao, S. Yang, C. Sun, Applied Catalysis B: Environmental 168–169 (2015) 448-457.
[5] S.-H. Li, Y. Zhao, J. Chu, W.-W. Li, H.-Q. Yu, G. Liu, Electrochimica Acta 92 (2013) 93-101.
[6] M. Kosmulski, Advances in Colloid and Interface Science 152 (2009) 14-25.
[7] M. Wang, J. Zai, X. Wei, W. Chen, N. Liang, M. Xu, R. Qi, X. Qian, CrystEngComm 17 (2015) 4019-4025.
[8] N.T. Hahn, V.C. Holmberg, B.A. Korgel, C.B. Mullins, The Journal of Physical Chemistry C 116 (2012) 6459-6466.
[9] T. Arai, Y. Konishi, Y. Iwasaki, H. Sugihara, K. Sayama, Journal of Combinatorial Chemistry 9 (2007) 574-581.
[10] R. Patil, S. Kelkar, R. Naphade, S. Ogale, Journal of Materials Chemistry A 2 (2014) 3661-3668.
[11] Y. Nakabayashi, M. Nishikawa, Y. Nosaka, Electrochimica Acta 125 (2014) 191-198.
[12] S.P. Berglund, H.C. Lee, P.D. Nunez, A.J. Bard, C.B. Mullins, Physical Chemistry Chemical Physics 15 (2013) 4554-4565.
[13] H.S. Park, C.-Y. Lee, E. Reisner, Physical Chemistry Chemical Physics 16 (2014) 22462-22465.
[14] A.A. Aref, A.A. Muneerah, D.M. Sun, H. Wang, C. Qing, Y.W. Tang, Materials Science in Semiconductor Processing 29 (2015) 262-271.
[15] W.-D. Oh, S.-K. Lua, Z. Dong, T.-T. Lim, Nanoscale 7 (2015) 8149-8158.
[16] E. Abdelkader, L. Nadjia, B. Ahmed, Journal of King Saud University - Science 27 (2015) 76-91.
[17] A. Muthukrishnaraj, S. Vadivel, I.M. Joni, N. Balasubramanian, Ceramics International 41 (2015) 6164-6168.
[18] A. Elaziouti, N. Laouedj, A. Bekka, R.-N. Vannier, Journal of King Saud University - Science 27 (2015) 120-135.
[19] E. Abdelkader, L. Nadjia, B. Ahmed, Applied Surface Science 258 (2012) 5010-5024.
[20] Y. Zhang, Y. Xie, J. Li, G. Yang, T. Bai, J. Wang, Journal of Alloys and Compounds 580 (2013) 172-175.
[21] Y. Deng, Y. Chen, B. Chen, J. Ma, Journal of Alloys and Compounds 559 (2013) 116-122.
[22] Y. Xie, Y. Zhang, G. Yang, C. Liu, J. Wang, Materials Letters 107 (2013) 291-294.
[23] M. Nishikawa, S. Hiura, Y. Mitani, Y. Nosaka, Journal of Photochemistry and Photobiology A: Chemistry 262 (2013) 52-56.
[24] Y. Deng, Y. Chen, B. Chen, J. Ma, ChemInform 44 (2013) no-no.
[25] T. Arai, M. Yanagida, Y. Konishi, Y. Iwasaki, H. Sugihara, K. Sayama, The Journal of Physical Chemistry C 111 (2007) 7574-7577.
[26] L. Wei, C. Shifu, Z. Sujuan, Z. Wei, Z. Huaye, Y. Xiaoling, J Nanopart Res 12 (2010) 1355-1366.
[27] Y. Liu, Y.C. Zhang, M. Zhang, Materials Letters 64 (2010) 1779-1781.
[28] M. Mohammadikish, CrystEngComm 16 (2014) 8020-8026.
[29] M.N. Nadagouda, R.S. Varma, Green Chemistry 8 (2006) 516-518.
[30] R.A. Sheldon, Green Chemistry 7 (2005) 267-278.
[31] W.-D. Oh, S.-K. Lua, Z. Dong, T.-T. Lim, Journal of Materials Chemistry A 2 (2014) 15836-15845.
[32] A.M. Abdulkarem, J. Li, A.A. Aref, L. Ren, E.M. Elssfah, H. Wang, Y. Ge, Y. Yu, Materials Research Bulletin 46 (2011) 1443-1450.
[33] L.S. Zhong, J.S. Hu, H.P. Liang, A.M. Cao, W.G. Song, L.J. Wan, Advanced Materials 18 (2006) 2426-2431.
[34] H. Cölfen, M. Antonietti, Angewandte Chemie International Edition 44 (2005) 5576-5591.
[35] H. Cölfen, S. Mann, Angewandte Chemie International Edition 42 (2003) 2350-2365.
[36] W. Yu, H. Xie, L. Chen, Y. Li, C. Zhang, Nanoscale Research Letters 4 (2009) 465-470.
[37] G. Cheng, H. Yang, K. Rong, Z. Lu, X. Yu, R. Chen, Journal of Solid State Chemistry 183 (2010) 1878-1883.
[38] B. Weintraub, Z. Zhou, Y. Li, Y. Deng, Nanoscale 2 (2010) 1573-1587.
[39] M. Frisch, T.G.W.U. Chemistry, Controlling the Hydrothermal Conditions to Synthesize Novel Uranium-based Heterometallic Coordination Polymers and Their Subsequent

Fluorescence Investigations, George Washington University, 2008.
[40] T. Sun, A.S. Teja, Journal of Chemical & Engineering Data 48 (2003) 198-202.
[41] H. Pang, F. Gao, Q. Lu, Chemical Communications (2009) 1076-1078.
[42] M. Chen, B. Wu, J. Yang, N. Zheng, Advanced Materials 24 (2012) 862-879.
[43] W.-D. Oh, Z. Dong, Z.-T. Hu, T.-T. Lim, Journal of Materials Chemistry A (2015).
[44] W. Zhang, H.L. Tay, S.S. Lim, Y. Wang, Z. Zhong, R. Xu, Applied Catalysis B: Environmental 95 (2010) 93-99.
[45] Y. Ren, L. Lin, J. Ma, J. Yang, J. Feng, Z. Fan, Applied Catalysis B: Environmental 165 (2015) 572-578.
[46] Y.-J. Lee, S. Kim, S.-H. Park, H. Park, Y.-D. Huh, Materials Letters 65 (2011) 818-820.
[47] B. Li, Y. Li, Y. Zhao, L. Sun, Journal of Physics and Chemistry of Solids 74 (2013) 1842-1847.
[48] S. Meghana, P. Kabra, S. Chakraborty, N. Padmavathy, RSC Advances 5 (2015) 12293-12299.
[49] K. Sunada, M. Minoshima, K. Hashimoto, Journal of Hazardous Materials 235–236 (2012) 265-270.